JOURNAL OF CATALYSIS 131, 523–544 (1991)

Bifunctional Reactions of Alkanes on Tungsten Carbides Modified by Chemisorbed Oxygen

ENRIQUE IGLESIA,*,[1] JOSEPH E. BAUMGARTNER,* FABIO H. RIBEIRO,† AND MICHEL BOUDART†

Corporate Research Laboratories, Exxon Research and Engineering Company, Route 22 East, Annandale, New Jersey 08801; and †Department of Chemical Engineering, Stanford University, Stanford, California 94305

Received March 15, 1991; revised June 3, 1991

Tungsten carbides modified by chemisorbed oxygen catalyze *n*-heptane isomerization with high selectivity. Kinetic, isotopic tracer, and deuterium-exchange measurements show that the reaction proceeds via sequential *n*-heptane dehydrogenation and heptene isomerization steps. At low temperatures, isomerization rates are limited by heptene rearrangements but dehydrogenation steps become increasingly rate-limiting as temperature increases. The isomer distribution in *n*-heptane and 3,3-dimethylpentane reaction products and the ^{13}C distribution in isoheptanes formed from *n*-heptane-1-^{13}C show that isomerization occurs predominantly by methyl migration steps typical of carbenium-ion rearrangements on acid sites. WO_x species on carbide surfaces appear to introduce acid sites similar to those present in supported tungsten oxides. *n*-Heptane dehydrocyclization and hydrogenolysis reactions also require heptene intermediates. Dehydrocyclization occurs predominantly by (1, 6) ring closure while hydrogenolysis leads to random cleavage of carbon–carbon bonds in *n*-heptane.

1. INTRODUCTION

Transition-metal carbides catalyze hydrocarbon conversion reactions at temperatures similar to those of supported noble metals (*1–5*). We recently reported a unique effect of chemisorbed oxygen on the alkane isomerization selectivity of tungsten carbide powders (*6, 7*). Chemisorbed oxygen inhibits alkane hydrogenolysis reactions that account for all the observed products on clean carbide samples. Oxygen adatoms also introduce a surface functionality that permits methyl-shift rearrangements of reactive alkene intermediates. Thus, oxygen-exposed tungsten carbides are apparently bifunctional; they catalyze alkane dehydrogenation and alkene rearrangements that also occur on conventional reforming catalysts.

Here, we describe the details of *n*-heptane rearrangement pathways by examining the effect of contact time on the product distribution; we also report isotopic tracers and deuterium-exchange studies that identify rate-limiting reaction steps and the intermediate role of heptene isomers in isomerization and dehydrocyclization reactions. We describe 3,3-dimethylpentane, methylcyclohexane, and *n*-heptane-1-^{13}C conversion data that support the presence of both dehydrogenation and methyl-shift sites on oxygen-exposed WC. Finally, we report the behavior of these materials at temperatures typical of catalytic reforming (>700 K), conditions that favor alkane dehydrocyclization reactions in catalytic reforming.

2. EXPERIMENTAL METHODS

2.1 Preparation and Characterization of Oxygen-Exposed WC Powders

High-surface-area tungsten carbide powders with WC structure were prepared by direct carburization of WO_3 (99.9994%, Johnson–Mathey puratronic grade) in CH_4/H_2 mixtures (*6*). Excess polymeric carbon was removed by a H_2 treatment at

[1] To whom correspondence should be addressed.

0021-9517/91 $3.00

973 K for 0.8 h. Previous studies showed that these fresh carbide samples chemisorb about 0.4 monolayers of CO and hydrogen; their carbide surfaces are equilibrated with stoichiometric bulk carbide phases and contain less than 0.10 monolayers of residual oxygen and no polymeric carbon (*6*).

The effect of chemisorbed oxygen on catalytic and chemisorptive properties was examined by exposing fresh carbides to O_2 at 300–800 K and then treating these samples in H_2 at 673 K. Fresh carbides were exposed to oxygen at room temperature (RT) by admitting O_2 into the cell slowly (0.1 μmol s^{-1} g^{-1}, 0.1- to 0.3-g sample, 70-cm^3 cell volume) in order to prevent exotherms and bulk conversion to WO_3. Oxygen uptakes were about 1 monolayer at RT. These samples were then heated to 800 K for about 0.25 h in O_2 (20 kPa) in order to increase the oxygen coverage that remains on the surface after a H_2 treatment (~0.5 monolayer). Samples exposed to O_2 are identified by the exposure temperature (e.g., WC/O-800 K). All chemisorption and catalytic data reported here were obtained on these oxygen-exposed WC samples. Similar data on fresh WC are reported elsewhere (*6, 7*).

CO chemisorption uptakes were measured at RT (*6*). Strongly adsorbed CO was used to calculate the surface site density on WC powders; similar site densities were obtained with H_2 or NH_3 as titrants (*6*). Specific surface areas were measured by N_2 physisorption at liquid nitrogen temperatures using the BET method (*8*). Surface characterization of fresh and oxygen-exposed WC by temperature-programmed reduction (TPR) and desorption (TPD) of preadsorbed NH_3 is described elsewhere (*6*).

A monofunctional Pt/SiO_2 catalyst was prepared by incipient wetness impregnation of SiO_2 (Davison 62, W. R. Grace Co.) with a solution of tetramminenitrate Pt(II) (Engelhard); it was then dried at 373 K for 12 h, calcined in air at 573 K for 0.5 h, and reduced in flowing H_2 by increasing the temperature from RT to 773 K at 0.1 K s^{-1} and holding for 4 h. The catalyst charge was 0.013 g. The Pt content, measured by atomic absorption, was 0.78 wt%. The Pt dispersion was determined by hydrogen titration of chemisorbed oxygen at RT (*9*).

The WO_3 on γ-Al_2O_3 support ($WO_3 \cdot Al_2O_3$) was prepared by incipient wetness impregnation of γ-Al_2O_3 (Engelhard, 185 m^2 g^{-1}) with a solution of ammonium metatungstate. The samples were dried at 100°C and calcined in air at 950°C for 15 h. Pt was then deposited by incipient wetness impregnation with a solution of chloroplatinic acid (Johnson–Mathey), dried at 100°C, and calcined (air, 450°C, 3 h). The sample (0.0205 g) was then charged into the reactor and reduced in flowing hydrogen at 400°C for 1 h before catalytic and chemisorption measurements. The Pt dispersion was determined by hydrogen chemisorption at RT (*6*).

2.2 Catalytic Measurements

Catalytic reaction studies were carried out in a gradientless recirculating batch reactor (reactor volume = 400 cm^3) (*10*). The WC/O-800 K catalyst charge was 0.024 g. Dihydrogen (Air Products, 99.995%) and dideuterium (Air Products, 99.5%) were purified by passing through a catalytic purifier (Engelhard) and a molecular sieve trap (13×, 77 K). Product samples were collected by sampling the gas phase in the reactor and analyzed by capillary column chromatography using flame ionization and mass spectrometric detection. At the end of an experiment, the products were collected in a cold (~77 K) 5-mm NMR tube containing deuterated chloroform.

Product concentrations are reported as turnovers, defined as the number of reactant molecules converted to a product per surface site; the site density was calculated from the irreversible CO or hydrogen uptakes at RT. Turnover rates are obtained from turnover–contact time plots. Initial turnover rates are given by the initial slope of such plots at very low reactant conver-

sion levels. Differential turnover rates are obtained from the local value of the slope at a given contact time or conversion level. Integral rates resemble those measured in fixed-bed reactors; they are given by the slope of the line connecting a given data point and the origin. We report these latter rates in the tables at low values of reactant conversion after at least 300 turnovers. Selectivities are reported as the percentage of the converted reactant that appears as a given product.

Unlabeled hydrocarbons were obtained from commercial sources (*n*-heptane, Fluka puriss grade, >99.5%; 1-heptene, Aldrich, >99%; 3,3-dimethylpentane, Wiley, >99.8%; methylcyclohexane, Fluka, 98%) and further purified by several freeze–pump cycles. *n*-heptane-1-^{13}C was prepared by the Cu-catalyzed coupling of *n*-hexylmagnesium bromide with $^{13}CH_3I$ in tetrahydrofuran (*10*). The isotopic purity at the terminal carbon position was greater than 99%.

2.3 Carbon-13 and Deuterium Isotopic Distribution Measurements

The ^{13}C content in individual reaction products and in unreacted feed was measured by mass spectrometry after being separated in a capillary column (Hewlett–Packard 5993 GC/MS, methylsilicone 50 m, 0.32-mm-diameter column). The deuterium content and the isotopic distribution were also measured by mass spectrometry using previously reported calculation procedures (*11*).

The isotopomer distribution in the products of *n*-heptane-1-^{13}C reactions was measured by ^{13}C NMR. NMR spectra were obtained on a JEOL GX-400 spectrometer operating at 100.54 MHz, using gated proton decoupling and a 5 to 20-s delay between acquisition pulses. Samples were mixed with deuterated chloroform and tetramethylsilane as an internal reference, and placed inside a 5-mm NMR tube. Chromium acetylacetonate was added in order to ensure complete relaxation of the ^{13}C nuclei between pulses. Integral data for each carbon position were corrected for natural abundance ^{13}C (*10*).

3. RESULTS/DISCUSSION

3.1 Catalyst Characterization

WC powders prepared by direct carburization of WO_3 did not chemisorb CO or hydrogen at RT. Removal of polymeric carbon by hydrogen at 973 K leads to surface sites that bind CO and H strongly (*7*). CO and H coverages on clean WC were 0.39–0.41 monolayers (Table 1; 1 monolayer $\cong 10^{15}$ cm^{-2}). TPR of fresh carbide samples in hydrogen leads to the evolution of CO above 1000 K, suggesting the presence of residual oxygen; this residual oxygen apparently resides in inaccessible regions of these samples, possibly as bulk oxycarbide species, or in strong oxygen binding sites at the surface. Weakly bound oxygen is removed predominantly as H_2O at much lower temperatures during TPR (*7*).

Exposure of fresh carbide samples to oxygen at RT does not affect surface area but decreases the number of surface sites that bind CO strongly (Table 1). This treatment introduces chemisorbed oxygen species that remain on the samples even after a hydrogen treatment at 673 K for 2 h. The extent of site blocking and the residual oxygen content increase with increasing oxygen exposure temperature. On WC/O-800 K, less than 10% of the strong binding sites initially present on fresh WC remain after oxygen exposure at 800 K and a subsequent H_2 treatment at 673 K; the residual oxygen coverage increases from 0.12 to 0.75 monolayers after such treatments (*7*).

The elemental composition and the metal dispersion of the supported Pt catalysts are also shown in Table 1.

3.2 n-Hexane Reactions on Fresh and Oxygen-Exposed WC

n-Hexane isomerization and hydrogenolysis areal rates on oxygen-exposed WC are shown in Fig. 1. Hydrogenolysis rates in-

TABLE 1

Elemental and Surface Characterization of Catalytic Materials

(a) WC powders	WC(1)	W/O-RT[a]	WC/O-800 K
BET Surface Area (m^2g^{-1})	30	30	30.7
CO chemisorption[b] uptake ($/10^{15}cm^{-2}$)	0.39	0.11	0.037
Oxygen Removed during H_2 TPR ($/10^{15}$ cm^{-2})	0.12	0.65	0.75
(b) Pt Catalysts Support:	SiO_2	$WO_3 \cdot Al_2O_3$	
Pt (%wt)[c]	0.78	0.33	
W (%wt)[c]	0	8.41	
(H/Pt) ratio[d]	0.80	0.20	

[a] Reference (*6*).
[b] 10^{15} cm^{-2} ~1 monolayer.
[c] By atomic absorption.
[d] By hydrogen chemisorption or hydrogen–oxygen titration.

crease linearly with increasing site density, suggesting that this reaction occurs on WC_x sites that bind CO and hydrogen strongly. The density of these sites decreases with increasing oxygen exposure temperature. Thus, chemisorbed oxygen inhibits hydrogenolysis reactions by decreasing the density of WC_x sites. In contrast, isomerization rates actually increase as WC_x site density decreases, suggesting that the rate-limiting step in the isomerization sequence does not require WC_x sites that chemisorb CO and H strongly. Chemisorbed oxygen introduces an isomerization function on the carbide surface; these WO_x surface sites are required for the rate-limiting step in the *n*-hexane isomerization sequence. Chemisorbed oxygen titrates WC_x sites and forms WO_x sites at the surface; as a result, isomerization rates and oxygen contents increase as the surface density of WC_x sites decreases.

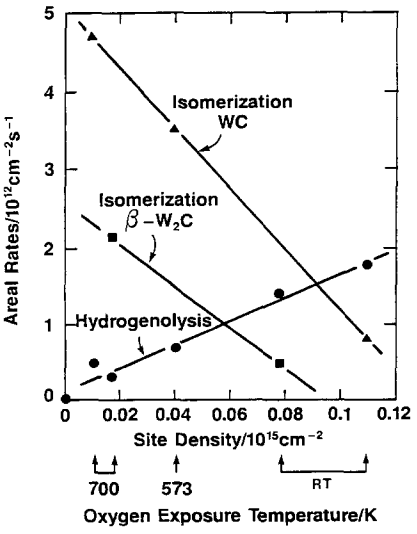

FIG. 1. *n*-Hexane isomerization and hydrogenolysis areal rates on oxygen-exposed WC (630 K, 6.1-kPa *n*-hexane, 95-kPa H_2, 5.0–25.4% conversion).

3.3 n-Heptane Conversion on WC/O—800 K and on Pt Catalysts

n-Heptane isomerization occurs with high selectivity on WC/O-800 K at 623 K (Fig. 2a, Table 2). Methylhexanes are the predominant isomers; 2-methylhexane and 3-methylhexane are formed in equal amounts, consistent with the statistical and thermodynamic methyl distribution in isoheptanes. Toluene and alkylcyclopentane

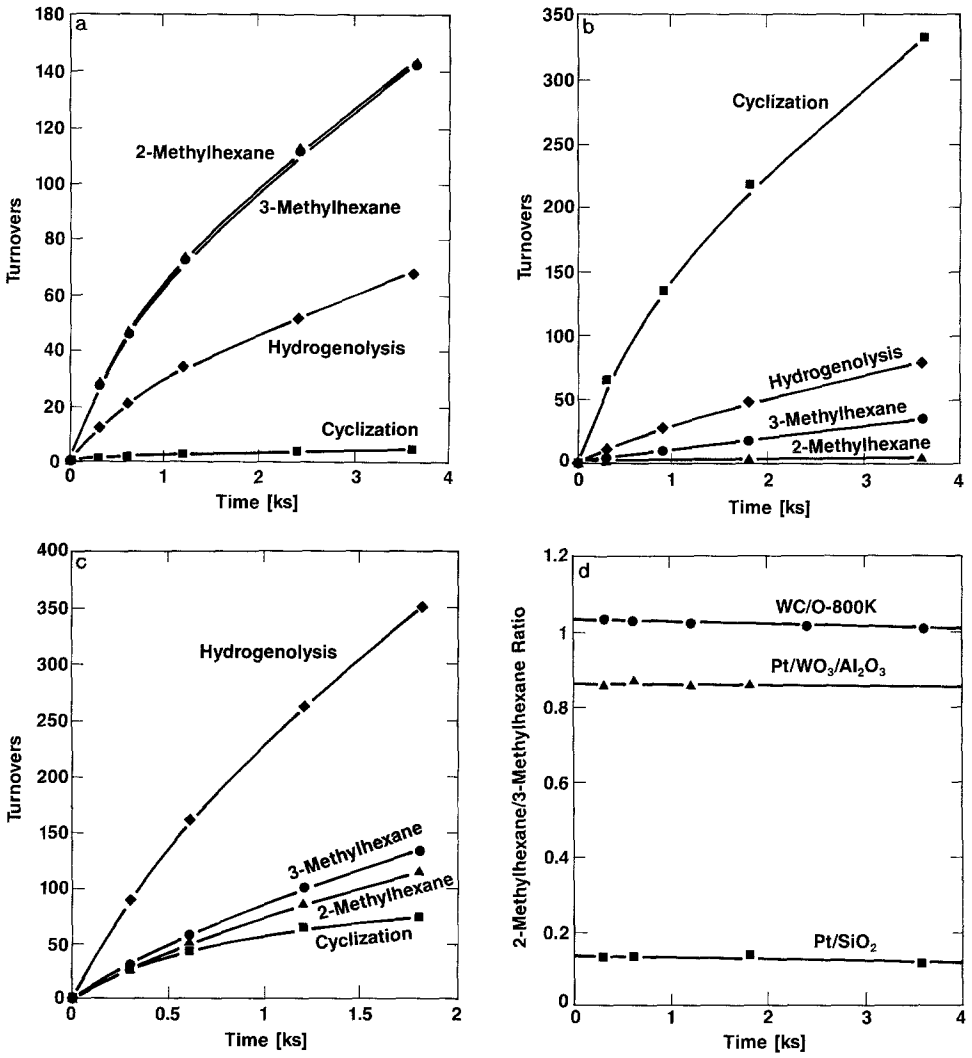

FIG. 2. *n*-Heptane isomerization, cyclization, and hydrogenolysis turnovers: (a) WC/O-800 K, (b) Pt/SiO_2, (c) $Pt/WO_3 \cdot Al_2O_3$, (d) 2-methylhexane/3-methylhexane isomer ratio (623 K, 4.4-kPa *n*-heptane, 96-kPa H_2, 5.0–25.4% conversion).

selectivities are low suggesting that (1, 5) and (1, 6) ring closure do not occur readily on WC/O-800 K at 623 K.

In contrast, monofunctional Pt/SiO_2 catalyzes cyclization reactions with high selectivity (Table 2, Fig. 2b). 3-Methylhexane is the predominant isomerization product and alkylcyclopentanes are reactive intermediates in the isomerization sequence. Isomerization occurs predominantly by hydrogenolysis of alkylcyclopentanes:

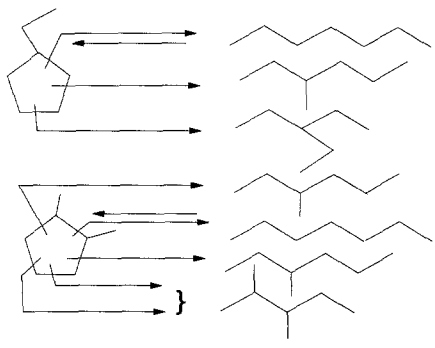

(1)

TABLE 2

Steady-State Turnover Rates (v_t) and Product Selectivity for *n*-Heptane Reactions on WC/O-800 K, Pt/SiO_2, and Pt/Al_2O_3 (623 K, 4.4-kPa *n*-Heptane, 96-kPa H_2)

	Catalyst		
	WC/O-800 K	Pt/SiO_2	$Pt/WO_3 \cdot Al_2O_3$
n-Heptane conversion (%):	12.9	10.5	13.4
$v_t(s^{-1})$	0.17	0.13	0.55
Reaction selectivity (%)			
Hydrogenolysis	16.3	14.7	47.9
Isomerization	79.5	14.1	35.5
Cyclization	0.7	67.4	13.5
Dehydrogenation	3.5	3.8	3.1
$\overline{X}^a$	1.59	1.02	1.07
Cracking pattern (%)[b]			
1–2 (Terminal)	32.8	27.9	15.7
2–3	30.4	23.0	22.0
3–4 (Mid-molecule)	36.8	49.1	62.4
Product selectivity (%)			
2-Methylhexane	37.3	0.75	14.9
3-Methylhexane	37.4	6.5	17.2
Ethylpentane	3.7	2.2	1.9
Dimethylpentanes	1.1	4.6	1.5
Alkylcyclopentanes	0.4	42.9	7.6
Toluene	0.3	23.7	5.9

[a] Average number of C–C bonds broken per reacted *n*-heptane molecule (Ref. (*6*)).

[b] Percentage of single-scission events leading to terminal (1–2), nonterminal (2–3), and mid-molecule (3–4) cleavage.

which leads preferentially to 3-methylhexane, 2,3-dimethylpentane, and ethylpentane products, the most abundant isomers on Pt/SiO_2 catalysts. On WC/O-800 K, however, the similar selectivity to 2-methyl and 3-methyl isomers, and the low 2,3-dimethylpentane, toluene, and alkylcyclopentane selectivities, suggest the absence of C_5-ring formation and hydrogenolysis pathways. Instead, it appears that methyl positions are rapidly isomerized; these rapid methyl shifts can occur readily during carbenium-ion rearrangements of methyl isomers:

(2)

because their interconversions do not require backbone rearrangements, chain lengthening, or primary carbenium-ion intermediates (*14*). Low-temperature methyl-shift isomerization via carbenium-ion species, however, requires protonation of alkene intermediates.

n-Heptane turnover rates are higher on $Pt/WO_3 \cdot Al_2O_3$ (0.55 s^{-1}) than on Pt/SiO_2 (0.13 s^{-1}) or WC/O-800 K (0.17 s^{-1}) (Table 2, Fig. 2c). However, hydrogenolysis is the predominant reaction (47.9% selectivity) and the cracking pattern strongly favors midmolecule cracking (Table 2). 2-Methylhexane and 3-methylhexane selectivities are similar and 2,3-dimethylpentane accounts for less than 1% of the products.

Therefore, isomerization proceeds predominantly by methyl shifts, consistent with the known acid properties of the $WO_3 \cdot Al_2O_3$ support (*12, 13*). Dehydrocyclization turnover rates on $Pt/WO_3 \cdot Al_2O_3$ (0.074 s^{-1}) and Pt/SiO_2(0.087 s^{-1}) are similar, suggesting that these reactions occur solely on Pt surface atoms in both supported catalysts.

The contributions of cyclic (Eq. (1)) and bond shift (Eq. (2)) pathways determine the ratio to 2-methyl to 3-methyl isomers among reaction products. Methyl-shift pathways give roughly equimolar amounts of the two isomers, but cyclic intermediates form only 3-methylhexane. Isomer ratios are near unity on WC/O-800 K (~1.05) and on $Pt/WO_3 \cdot Al_2O_3$ (~0.86) (Fig. 2d). The slight excess of 3-methylhexane in the latter reflects a cyclic contribution to isomer products by the Pt sites on the bifunctional catalyst. In contrast, cyclic isomerization pathways account for most of the product on monofunctional Pt/SiO_2 and the isomer ratio is quite small (0.13).

Isomer distributions on WC/O-800 K and $Pt/WO_3 \cdot Al_2O_3$ are very similar and suggest a mechanistic resemblance in isomerization pathways. However, hydrogenolysis rates and selectivity, bond cleavage patterns, and the average number of carbon–carbon bonds broken in a surface sojourn differ markedly on these two catalysts. The random cleavage and multiple hydrogenolysis selectivity observed on WC/O-800 K reflect chemistry on strong-binding WC_x surface sites (*6*). In contrast, single scission of nonterminal carbon–carbon bonds is typical of acid-catalyzed cracking reactions on strong acid sites because of the higher stability of substituted carbenium ions and because cracking rates decrease rapidly as molecular size decreases (*14*).

Acid-catalyzed cracking is slow on WC/O-800 K. Sites capable of methyl-shift rearrangements of reactive intermediates exist on tungsten carbide surfaces modified by chemisorbed oxygen; they catalyzed isomerization with high selectivity, without concomitant acid cracking. The presence of acid sites on such oxygen-modified carbide surfaces was previously demonstrated by NH_3 TPD studies (*6*).

Brønsted acid sites are introduced into Al_2O_3 surfaces that normally contain only weak Lewis sites by the presence of small WO_x crystallites with tetrahedral coordination of tungsten atoms (*13*). The density and acid strength of such Brønsted sites are much greater than those on large WO_3 crystallites, which contain W atoms only in octahedral sites. Brønsted acid sites can form stable carbenium ions by protonation of alkenes; apparently, such acid sites cannot abstract hydride ions from alkanes and they require alkenes as intermediates or as initiators of carbenium-ion chain reactions typical of Friedel–Crafts metal halide catalysts (*14*). Thus, the presence of dehydrogenation sites is required for isomerization to proceed. In what follows, we show that WO_x acid sites catalyze the formation of isoheptanes and isoheptenes by secondary rearrangements of intermediate alkenes.

3.4 Dehydrogenation Reaction Steps on WC/O—800 K and Pt Catalysts

Heptenes are formed during reactions of *n*-heptane on WC/O-800 K. Site yields for all linear heptene isomers (1-, *trans*-2-, *cis*-2-, *trans*-3-, and *cis*-3-heptenes) initially increase with increasing contact time but reach constant values quickly (~0.3 ks) (Fig. 3a). Similar trends occur on Pt/SiO_2 and $Pt/WO_3 \cdot Al_2O_3$, but initial dehydrogenation site–time yields are much higher than those on WC/O-800 K (Fig. 3a). The constant turnover values observed for all heptene isomers are typical of intermediate products in a reaction sequence

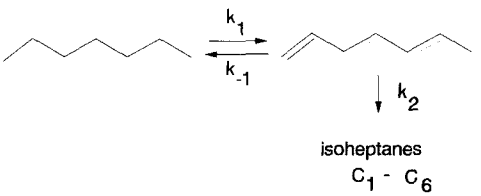

(3a)

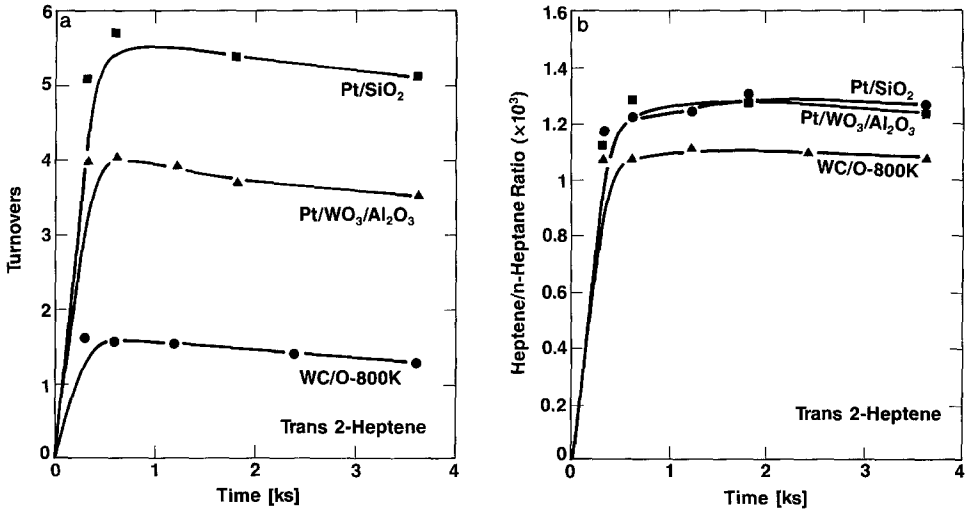

FIG. 3. Heptene turnovers and selectivity during *n*-heptane reactions: (a) *trans*-2-heptene turnovers, (b) *trans*-2-heptene/*n*-heptane ratio (623 K, 4.4-kPa *n*-heptane, 96-kPa H_2, 5.0–25.4% *n*-heptane conversion).

where the rate constants (k_i) include any hydrogen concentration dependence required to describe each rate. Steady-state heptene to heptane ratios are given by

$$R = \frac{(\text{heptene})}{(n\text{-heptane})} = \frac{k_1}{k_{-1} + k_2}; \quad (3b)$$

they approach a value of k_1/k_2 for an irreversible dehydrogenation step ($k_{-1} \ll k_2$) and a value of k_1/k_{-1} when such a step is quasi-equilibrated ($k_{-1} \gg k_2$). In the latter case, the heptene to heptane ratios equal their equilibrium values.

At steady state, heptene/*n*-heptane ratios on all catalysts approach their equilibrium values (Fig. 3b). Thus, dehydrogenation–hydrogenation steps are fast and quasi-equilibrated on all catalysts at 623 K. On WC/O-800 K, *trans*-2-heptene to *n*-heptane ratios (1.05×10^{-3}) are slightly lower than those on Pt (1.23×10^{-3}), suggesting that equilibration is not quite complete; this is consistent with the initial dehydrogenation rates on WC/O-800 K being lower than those on Pt (Fig. 3b). The deviation from equilibrium suggests that k_{-1}/k_2 is about 5.8 on WC/O-800 K; it is greater than 50 on Pt-containing catalysts. Double-bond migration is also very rapid; all linear heptene isomers reach equilibrium values. Isomerization rates are apparently limited by subsequent reactions of this equilibrated pool of heptene intermediates.

These results are consistent with an intermediate role of alkenes in isomerization reactions on WC/O-800 K. Yet, we cannot rule out that alkenes are unreactive spectator species that equilibrate quickly with *n*-heptane but do not convert further to stable isomerization, cyclization, or hydrogenolysis products. Therefore, we measured directly the contribution of these heptene intermediates to *n*-heptane isomerization on WC/O-800 K by measuring the isotopic content in each product of *n*-heptane-1-^{13}C/1-heptene reaction mixtures.

3.5 Isotopic Tracer Studies of n-Heptane Isomerization Pathways

Isotopic tracer studies of *n*-heptane-1-^{13}C/1-heptene mixtures (73%/27%) probe the reversibility of the dehydrogenation steps and the intermediate role of alkenes in *n*-heptane isomerization reactions. In effect, we can determine the relative contributions of direct *n*-heptane isomerization

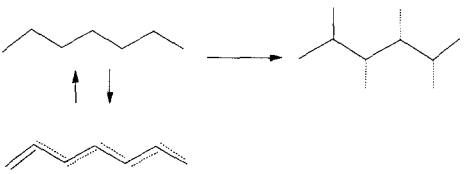

(4)

and of alkene-mediated isomerization

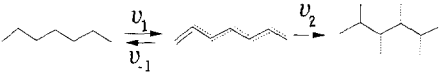

(5)

by measuring the rate of appearance of labeled (from *n*-heptane-1-^{13}C and unlabeled (from 1-heptene) products.

These studies show that alkenes are reactive intermediates in *n*-heptane isomerization. Initial isomer products contain almost no ^{13}C suggesting that they are predominantly formed from unlabeled 1-heptene reactants (Fig. 4a). Heptane–heptene isotopic scrambling occurs quickly and unreacted heptane rapidly attains its equilibrium ^{13}C fraction (~0.75). The ^{13}C content of *n*-butane (0.22), *n*-pentane (0.23), and *n*-hexane (0.23) products is low even after 1.8-ks contact times and significant *n*-heptane conversion (~10%). Thus, it appears that the formation of C_1–C_6 products also requires alkene intermediates.

Turnovers of labeled and unlabeled 2-methylhexane clearly show that isomerization of 1-heptene occurs more rapidly than that of *n*-heptane (Fig. 4b). The initial slope of unlabeled 2-methylhexane site yield plots is initially large and then decreases rapidly because of isotopic dilution of the unlabeled alkene intermediates by dehydrogenation of labeled *n*-heptane. In contrast, the initial slope of 2-methylhexane-^{13}C products is initially zero, suggesting the absence of direct alkane isomerization pathways and the requirement for an initial increase in (^{13}C) alkene intermediates. The ratio of ^{13}C-labeled to unlabeled isohexane products extrapolates to a value less than 0.005 for both 2-methyl and 3-methyl isomers (Fig. 4b). Therefore, we conclude that heptene isomerization is more than 200 times faster than direct isomerization of *n*-heptane.

The relative rates of heptene hydrogenation (v_{-1}) and of its conversion to stable products (v_2) can be estimated from unlabeled *n*-heptane ($n^{12C}_{[n\text{-heptane}]}$) and stable products ($n^{12C}_{[\text{products}]}$) turnovers:

$$\frac{v_{-1}}{v_2} = \frac{n^{12C}_{[\text{n-heptane}]}}{n^{12C}_{[\text{products}]}} = \frac{k_{-1}}{k_2}. \qquad (6)$$

This ratio extrapolates to a value of 6.1 ± 0.3 at zero contact time and 623 K (Fig. 4c); it agrees well with k_{-1}/k_2 values estimated previously from the observed deviations from equilibrium heptene to heptane ratios (5.8). Therefore, dehydrogenation–hydrogenation steps are nearly equilibrated during *n*-heptane isomerization on WC/O-800 K at 623 K. In contrast, similar tracer studies of *n*-heptane-1-^{13}C/1-heptene mixtures showed that k_{-1}/k_2 ratios are greater than 50 on Pt/SiO_2.

Thus, we conclude that dehydrogenation steps are quasi-equilibrated on WC/O-800 K and that the rate-limiting step involves isomerization and cracking of alkene intermediates. In what follows, we show that skeletal rearrangements of these alkene intermediates involve methyl-shift steps, as already suggested by the similar selectivity to 2-methylhexane and 3-methylpentane on WC/O-800 K. We describe isotopomer distributions in the products of *n*-heptane-1-^{13}C isomerization and initial isomer products of 3,3-dimethylpentane reactions that are consistent with methyl-shift isomerization pathways.

3.6 Isotopomer Distribution in n-Heptane-1-^{13}C Reaction Products

The products of the isomerization of *n*-heptane-1-^{13}C on WC/O-800 K contain ^{13}C only in terminal carbon positions (Table 3), consistent with methyl-shift rearrangement steps:

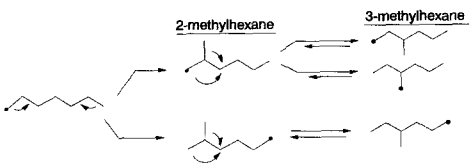

(7)

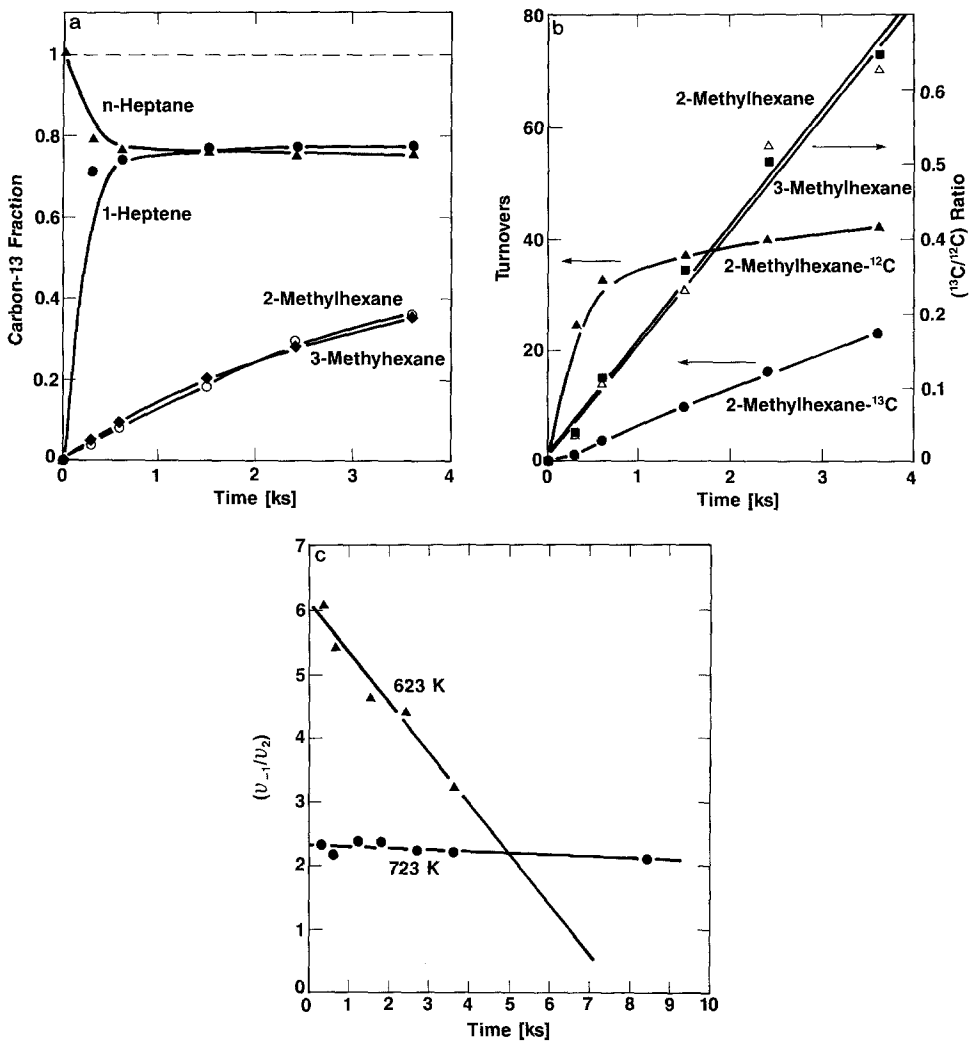

FIG. 4. Reactions of 1-heptene/*n*-[1-^{13}C]heptane mixtures on WC/O-800 K: (a) ^{13}C content of reactants and products, (b) turnovers and fraction of isoheptanes formed from *n*-heptane-1-^{13}C, (c) olefin hydrogenation/isomerization rates (623 K, 723 K) (623 K, 4.4-kPa hydrocarbons, 95-kPa H_2, 27.8% 1-heptene, 72.2% *n*-heptane-1-^{13}C, 5.9–10.7% net *n*-heptane conversion).

Rapid methyl shifts ultimately lead to identical ^{13}C enrichment at all terminal positions, without the incorporation of ^{13}C into nonterminal carbons. For example, ^{13}C NMR intensities of peaks corresponding to the 1-position (0.66) and 7-positions (0.55) in 3-methylhexane are similar (Table 3).

Some enrichment occurs at nonterminal positions in *n*-heptane, apparently as a result of chain lengthening of isoheptanes. Internal carbons in 3-methylhexane and ethylpentane, however, are not enriched; thus, isomerization does not involve C_5-ring intermediates. Such rearrangements would lead to significant enrichment at internal carbons in methylhexanes, ethylpentane, and *n*-heptane:

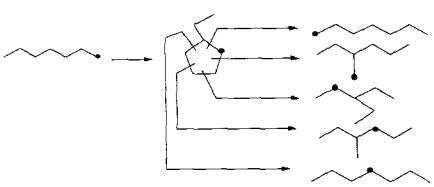

(8)

TABLE 3

Isotopomer Distribution in *n*-Heptane-1-^{13}C Reaction Products (623 K, 4.4-kPa *n*-Heptane-1-^{13}C, 96-kPa H_2, 10.8% *n*-Heptane Conversion)

Product (position)	NMR Integrated intensity (arb. units)[a]
2-Methylhexane	
(1,7)	0.95
(2)	0
(3)	0
(4)	0
(5)	0
(6)	[b]
3-Methylhexane	
(1)	0.66
(2)	0
(3)	0
(4)	0
(5)	0
(6)	[b]
(7)	0.55
Ethylpentane	
(1,5,7)	0.31
(2,4,6)	0
(3)	0
n-Heptane	
(1,7)	90.0
(2,6)	0.79
(3,5)	0.40
(4)	0.17

[a] Corrected for natural abundance ^{13}C.

[b] NMR peaks overlap with enriched 1-position in unreacted *n*-heptane-1-^{13}C.

The products of *n*-heptane-1-^{13}C isomerization contain one ^{13}C atom per molecule. Thus, isomerization occurs without the formation of *n*-heptane oligomers and involves only one *n*-heptane molecule. *n*-Heptane reactions on WC/O-800 K do not involve intermolecular isotopic exchange reactions steps, previously reported during alkane and alkene (*15–17*) reactions on strong solid acids. No unlabeled *n*-heptane or other unlabeled C_7 molecules were detected among the products of *n*-heptane-1-^{13}C reactions; thus, isotopic exchange between labeled hydrocarbons and carbidic (^{12}C) surface carbon does not occur during catalytic reactions on WC/O-800 K.

3.7 3,3-Dimethylpentane Isomerization on WC/O—800 K and Pt-Based Catalysts

3,3-Dimethylpentane isomerizes via alkene (3,3-dimethyl-1-pentene) intermediates on acid sites. Isomerization occurs by skeletal rearrangements of carbenium-ion intermediates that lead to 2,3-dimethylpentane as the initial isomeric product (*6*). Cracking occurs by β-scission, only after isomerization of the initial carbenium-ion species:

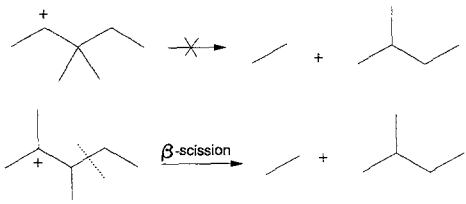

(9)

3,3-Dimethylpentane is a sensitive molecular probe of isomerization pathways (*6, 10*). The isomer distribution differs among carbonium-ion pathways, C_5-ring hydrogenolysis processes, typical of highly dispersed Pt (*18*), and metallacyclobutane bond-shift mechanisms (*19*). Thus, 2,2-dimethylpentane and 2-methylhexane are the predominant products of C_5-ring hydrogenolysis pathways, while metallacyclobutane pathways give approximately equal amounts of 2,3-dimethylpentane and ethylpentane isomers. Carbenium-ion rearrangements also give 2,3-dimethylpentane as a predominant product but without concurrent formation of ethylpentane. Instead, these pathways rapidly isomerize 2,3-dimethylpentane to 2,4-dimethylpentane by rapid methyl shifts in carbenium ion.

Acid-catalyzed cracking of 3,3-dimethylpentane gives predominantly ethane and isopentane on bifunctional Pt/$WO_3 \cdot Al_2O_3$ catalysts. Cracking selectivity is high (~70%) because of the long residence time of carbenium ions on strong acid sites present in the $WO_3 \cdot Al_2O_3$ support. Thus, 2,3-dimethylpentane ions tend to undergo β-scission before they desorb as isomer

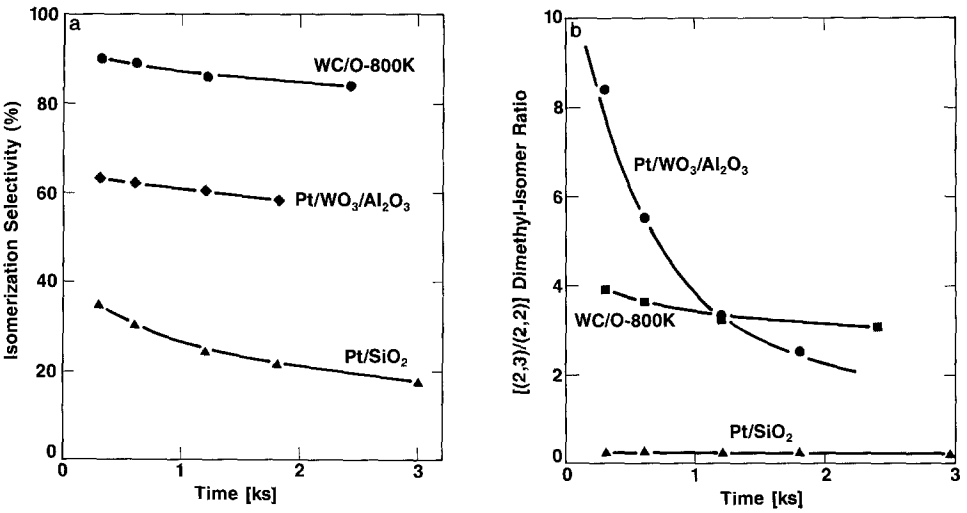

FIG. 5. 3,3-Dimethylpentane reactions on WC/O-800 K, Pt/SiO_2, and $Pt/WO_3 \cdot Al_2O_3$. (a) Isomerization selectivity, (b) 2,3-dimethylpentane to 2,2-dimethylpentane product ratio (623 K, 4.4-kPa 3,3-dimethylpentane, 96-kPa H_2, < 10% conversion).

products. 3,3-Dimethylpentane isomerization selectivity is higher on WC/O-800 K than on Pt/SiO_2 or $Pt/WO_3 \cdot Al_2O_3$ (Fig. 5a). On WC/O-800 K and Pt/SiO_2, cracking probabilities for terminal and nonterminal carbon–carbon bonds are similar. On $Pt/WO_3 \cdot Al_2O_3$, nonterminal cracking is about eight times faster than terminal cracking and ethane and isopentane are the predominant hydrogenolysis products.

The ratio of (2,3) to (2,2) isomers among 3,3-dimethylpentane reaction products reflects the relative contributions of methyl-shift and cyclic isomerization pathways. This ratio is very high on $Pt/WO_3 \cdot Al_2O_3$ (Fig. 5b), suggesting that isomerization occurs predominantly by methyl-shift rearrangements. On WC/O-800 K, this ratio is also large (~4) but decreases with increasing contact time because of the rapid secondary conversion of 2,3-dimethylpentane to 2,4-dimethylpentane. These results suggest that alkane isomerization occurs predominantly by methyl shifts of carbenium ions on WC/O-800 K.

Ring-closure reactions of 3,3-dimethylpentane occur very slowly on WC/O-800 K (1,1-dimethylcyclopentane <0.2%). Dimethylcyclopentane selectivities are much higher on Pt-containing catalysts ($Pt/WO_3 \cdot Al_2O_3$, 6.9–7.8%; Pt/SiO_2, 10.3–18.5%), which also catalyze the formation of toluene directly from 3,3-dimethylpentane. In contrast with Pt-based catalysts, WC/O-800 K catalysts lack ring-closure sites required in dehydrocyclization reactions and in isomerization pathways involving C_5-ring intermediates.

3.8 Methylcyclohexane Reactions on WC/O-800 K and on Pt Catalysts

Methylcyclohexane dehydrogenates to toluene on metals and isomerizes to alkylcyclopentanes on bifunctional catalysts via methylcyclohexene intermediates (*14*). Both dehydrogenation and isomerization of methylcyclohexane occur on WC/O-800 K (Fig. 6, Table 4), suggesting the presence of acid sites. In contrast, only dehydrogenation products are detected on $Pt/WO_3 \cdot Al_2O_3$ catalysts. Methylcyclohexane and methylcyclohexene dehydrogenation rates are much lower on WC/O-800 K than on Pt-containing catalysts (Table 4); methylcyclohexene concentrations are near equilibrium on WC/O-800 K and isomeriza-

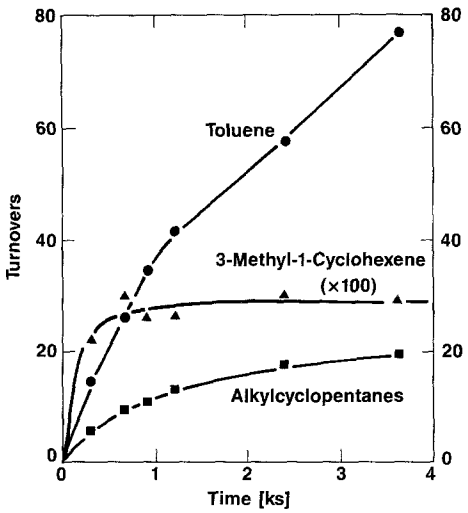

FIG. 6. Methylcyclohexane reactions on WC/O-800 K. Toluene, alkylcyclopentane, and 3-methyl-1-cyclohexene turnovers (623 K, 0.33-kPa methylcyclohexane, 96-kPa H_2, 9.8–36% methylcyclohexane conversion).

tion rates are limited by reactions of these unsaturated intermediates on WC/O-800 K.

Contact time effects on 3-methylcyclo-1-hexene turnovers also suggests the cycloalkenes are reactive intermediates on WC/O-800 K (Fig. 6). Methylcyclohexenes are not detected on Pt-based catalysts, because of their rapid dehydrogenation to toluene in subsequent steps. These secondary dehydrogenation steps prevent isomerization of cycloalkene intermediates on WO_3–Al_2O_3 acid sites and maintain steady-state methylcyclohexene concentrations well below equilibrium values.

TABLE 4

Turnover Rates (ν_t) and Product Selectivity for Methylcyclohexane Reactions on WC/O-800 K and Pt/SiO_2 (623 K, 3.3-kPa Methylcyclohexane, 97-kPa H_2)

	Catalyst	
	WC/O-800 K	Pt/SiO_2
Methylcyclohexane conversion (%):	23.7	37.0
$\nu_t(s^{-1})$:	0.048	12.0
Product selectivity (%)		
Toluene	66.3	99.7
Alkylcyclopentanes	17.9	0
Heptanes	11.1	0.02
C_1–C_6	5.0	0.27

3.9 Temperature Effects on Selectivity, Reaction Pathways, and Deactivation (WCO-800 K)

WC powders modified by chemisorbed oxygen were also tested at higher temperature (723 K), conditions that favor dehydrocyclization, and dehydrogenation reactions typical of catalytic reforming. At these conditions, catalyst deactivation was initially fast, but turnover rates reached a constant value (0.065–0.070 s^{-1}, Table 5) after about 100 turnovers. Steady-state *n*-heptane conversion rates and selectivities at 723 K, after this initial deactivation period, are reported in Table 5.

Dehydrocyclization (5.3%) and dehydrogenation (27.8%) selectivities at 723 K are much higher than at 623 K (1.2 and 3.5%, respectively); turnover rates (0.069 s^{-1}, based on fresh catalyst site density), however, are actually lower than their value at 623 K (0.17 s^{-1}), because of the rapid initial deactivation at higher temperatures. Multiple hydrogenolysis probabilities ($\bar{X}$) and random-bond cleavage patterns are similar at 623 and 723 K. 2-Methylhexane and 3-methylhexane isomers are formed in equimolar amounts, as also observed in methyl-shift rearrangements at 623 K (Table 5, Fig. 7a).

Heptene turnovers initially increase but approach steady-state heptene to *n*-heptane ratios much more slowly than at 623 K (Fig. 7b). These ratios are well below equilibrium values at 723 K. Steady-state alkene/alkane ratios for *trans*-2-heptene (0.0185), *cis*-2-heptene (0.0105), and 1-heptene (0.0082) are much higher than at 623 K but about a factor of 0.67–0.70 lower than equilibrium ratios for all heptene isomers (0.0271,

TABLE 5

Reaction Temperature Effects on *n*-Heptane Turnover Rates and Selectivity (WC/O—800 K) (4.4-kPa *n*-Heptane, 97-kPa H_2)

	Reaction temperature (K)		
	623	723	623[a]
n-Heptane conversion (%):	12.9	11.7	12.4
$v_t(s^{-1})$	0.17	0.069	0.020
Reaction selectivity (%)			
Hydrogenolysis	16.3	44.6	34.3
Isomerization	79.0	22.3	60.7
Cyclization	1.2	5.3	1.2
Dehydrogenation	3.5	27.8	3.8
$\bar{X}$[b]	1.59	1.69	1.10
Cracking pattern (%)[c]			
1–2 (Terminal)	32.8	32.9	30.8
2–3	30.4	34.2	35.2
3–4 (Mid-molecule)	36.8	32.9	34.0
Product selectivity (%)			
2-Methylhexane	37.3	7.2	26.0
3-Methylhexane	37.4	7.0	30.1
Ethylpentane	3.7	1.6	2.6
Dimethylpentanes	1.1	1.5	1.9
Alkylcyclopentanes	0.4	0.5	0.8
Toluene	0.8	4.8	0.5

[a] After *n*-heptane reactions at 723 K.

[b] Average number of C–C bonds broken per reacted *n*-heptane molecule (Ref. (*6*)).

[c] Percentage of single-scission events leading to terminal (1–2), nonterminal (2–3), and mid-molecule (3–4) cleavage.

0.015, 0.0061, respectively). These values suggest that k_{-1}/k_2 is about 2.1 at 723 K (Eq. (3b)); its value at 623 K is higher (5.8). The similar deviation from equilibrium for all heptene isomers does not reflect similar k_{-1}/k_2 ratios for all double-bond positions. Instead, it arises from rapid double-bond migration in the heptene isomer pool before subsequent isomerization steps.

As temperature increases, the initial dehydrogenation step becomes increasingly rate-limiting. This trend reflects an activation energy for heptene isomerization higher than that for *n*-heptane dehydrogenation; it is not caused by selective deactivation of WC_x dehydrogenation sites at high temperatures, because *n*-heptane reactions at 623 K, after deactivation at 723 K for 5–6 h, give k_{-1}/k_2 ratios that are actually higher ($k_{-1}/k_2 = 8$) than before deactivation. This slight increase suggests that WO_x, rather than WC_x sites, are more rapidly deactivated at higher temperatures.

n-Heptane conversion rates at 623 K are significantly lower after deactivation at 723 K (0.02 s^{-1} vs 0.17 s^{-1}; Table 5). The isomer distribution, however, is unaffected. Hydrogenolysis selectivity increases, suggesting again that WC_x sites, apparently responsible for this reaction, are less deactivated than isomerization sites during high-temperature catalysis. Multiple

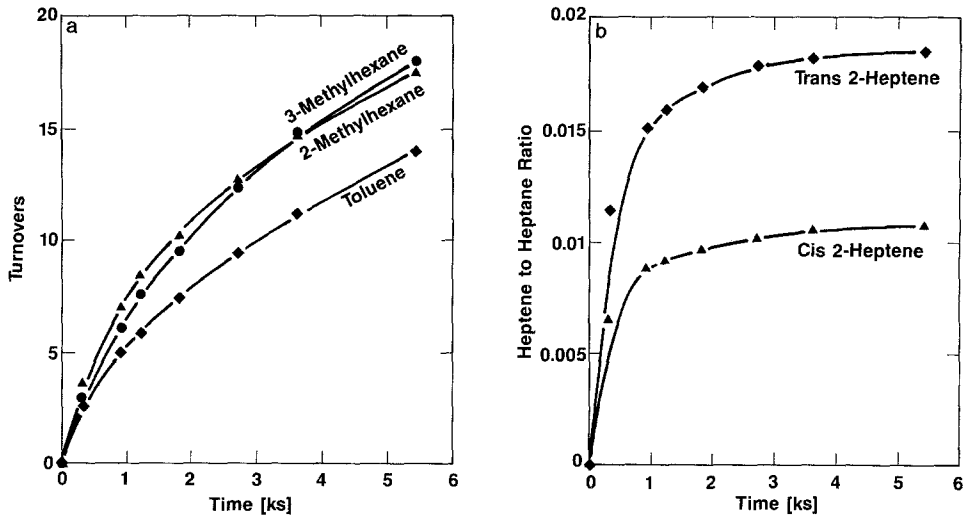

FIG. 7. *n*-Heptane reactions on WC/O-800 K: (a) Toluene and isoheptane turnovers, (b) heptene/*n*-heptane ratios (723 K, 4.4-kPa *n*-heptane, 96-kPa H_2, 5–12.8% *n*-heptane conversion).

hydrogenolysis events, however, are less likely on deactivated catalysts. As we reported previously, stronger binding sites that catalyze such deep hydrogenolysis events are more readily deactivated by carbonaceous deposits on tungsten carbides (*7*).

3.10 1-Heptene/n-[1-^{13}C]Heptane Reactions on WC/O-800 K (723 K)

The isotopic content of the products of 1-heptene/*n*-heptane-1-^{13}C reactions on WC/O-800 K at 723 K is shown in Fig. 8a. Hydrogenation of unlabeled 1-heptene and of its rapidly equilibrated isomers leads to an initial decrease in the ^{13}C content of *n*-heptane. Therefore, the initial dehydrogenation step in *n*-heptane reactions on WC/O-800 K remains reversible at 723 K. However, the rate of isotopic dilution of *n*-heptane is much slower than that at 623 K.

All heptene isomers have similar isotopic composition because their interconversion is fast compared with subsequent heptene conversion to products (Fig. 8a). The initial toluene products are unlabeled; they are preferentially formed from the unlabeled heptene pool, rather than from the more abundant *n*-heptane-1-^{13}C reactant. Unlabeled toluene turnovers increase rapidly with contact time; the slope of unlabeled toluene turnover plots then decreases as the unlabeled heptene pool is enriched with ^{13}C by on-going dehydrogenation of *n*-heptane-1-^{13}C (Fig. 8b). In contrast, [^{13}C]-toluene turnover plots show an initial zero slope; after the concentration of ^{13}C-labeled heptenes reaches steady-state values, the slope also reaches a constant value. The ratio of labeled to unlabeled isoheptanes and toluene (and also for cracking products) extrapolates to values less than 0.003 at zero contact time (Fig. 8b). Thus, the rate of 1-heptene conversion to these products is 300 times faster than that of *n*-heptane, in spite of its lower concentration in the reactant pool (26.5% 1-heptene, 73.5% *n*-heptane-1-^{13}C).

The ratio of heptene hydrogenation to conversion turnovers on WC/O-800 K is much lower at 723 K ($k_{-1}/k_2 = 2.3 \pm 0.2$) than at 623 K ($k_{-1}/k_2 = 6.1 \pm 0.3$) (Fig. 4c), consistent with the greater deviation from equilibrium heptene/*n*-heptane ratios observed at higher temperatures. These data support our previous conclusion that the

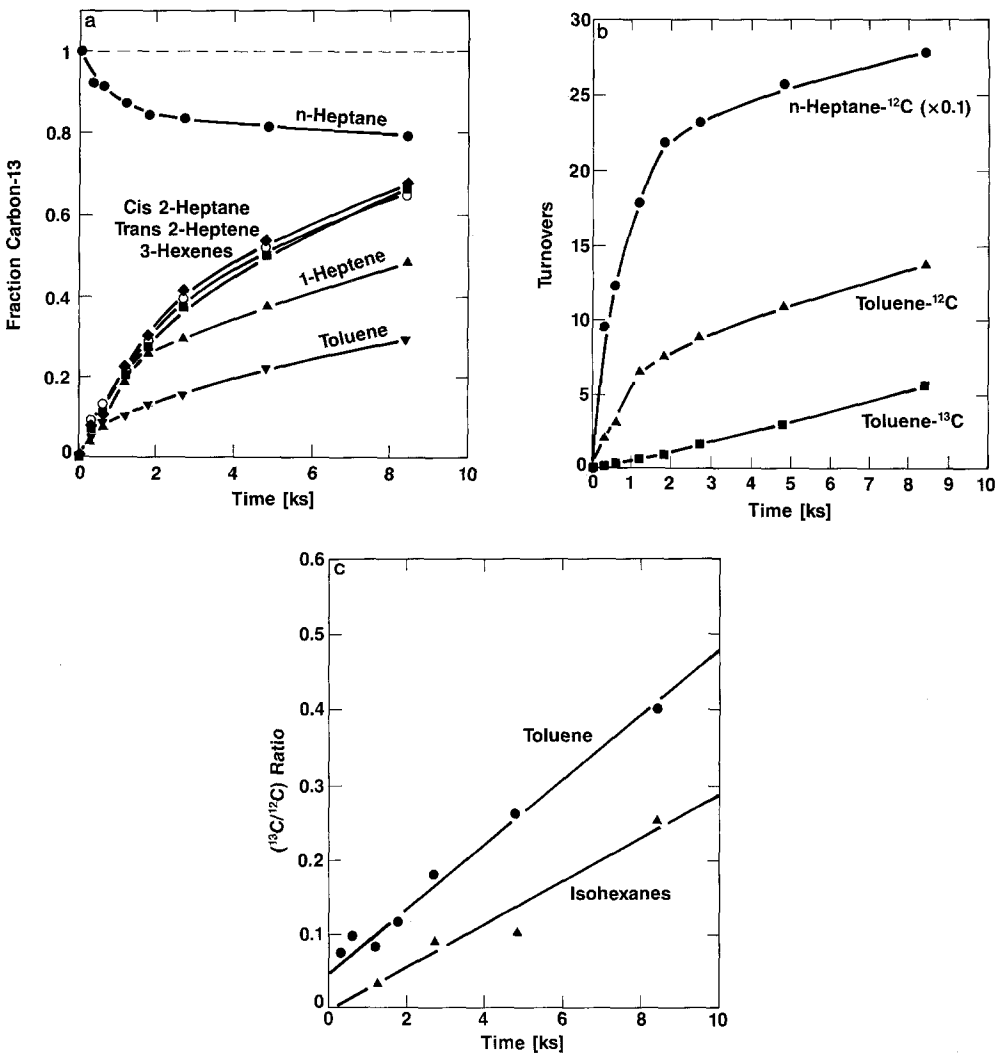

FIG. 8. Reactions of 1-heptene/*n*-heptane-1-^{13}C mixtures on WC/O-800 K: (a) ^{13}C content in reactants and products, (b) turnovers, (c) fraction of toluene and isoheptanes formed from *n*-heptane-1-^{13}C (723 K, 4.4-kPa hydrocarbons, 96-kPa H_2, 26.5% 1-heptene/73.5% *n*-heptane-1-^{13}C, ≤ 15.0% net conversion).

initial dehydrogenation step becomes increasingly irreversible (i.e., rate-limiting) at higher temperatures. The k_{-1}/k_2 values obtained at 723 K from isotopic measurements (2.3 ± 0.2) are in excellent agreement with those calculated from the differences between steady-state and equilibrium alkene/alkane ratios (2.1).

The isotopomer distribution in the toluene and isoheptane products of *n*-heptane-1-^{13}C reactions on WC/O-800 K at 723 K was measured by ^{13}C NMR. The results are shown in Table 6. ^{13}C enrichment occurs only at terminal carbons in isoheptanes suggesting that isomerization does not proceed via hydrogenolysis of cyclic intermediates. All carbon atoms in toluene molecules are enriched (Table 6). Methyl and *ortho*-carbons are preferentially enriched (49.8 and 37.7% ^{13}C, respectively). *Meta*-, *para*-, and

TABLE 6

Isotopomer Distribution in Products of *n*-Heptane-1-^{13}C Reactions on WC/O-800 K (723 K, 4.4-kPa *n*-Heptane, 97-kPa H_2, 27.5% Conversion)

Product (position)	Experimental[a]	Percentage of product molecule with ^{13}C at indicated positions: Predicted from thermal heptatriene cyclization[b]	Predicted from heptatriene model and methyl shifts[c]
		Toluene	
Methyl-	49.8	47.3	47.3
Ortho-	37.7	48.6	40.9
Meta-	5.9	2.7	6.2
Para-	3.8	1.4	3.3
Ipso-	2.8	0	2.2
		2-Methylhexane	
(1,7)	71.0	—	—
(2)	0	—	—
(3)	0.9	—	—
(4)	0	—	—
(5)	0	—	—
(6)	28.1	—	—

[a] Corrected for natural abundance ^{13}C.

[b] Thermal cyclization of equilibrated mixture of conjugated and nonconjugated heptatrienes (*10*).

[c] Predicted from Footnote *b* followed by rapid secondary isotopomerization (methyl shifts) of 25% of the toluene molecules.

ipso-positions in toluene show similar enrichment per carbon atom (2.95, 3.8, 2.8%, respectively). About half of the ^{13}C atoms lie within the toluene ring (50.2%) and the remaining half (49.8%) in the methyl group.

The toluene isotopomer distribution is consistent with direct (1,6) or (2,7) ring-closure pathways:

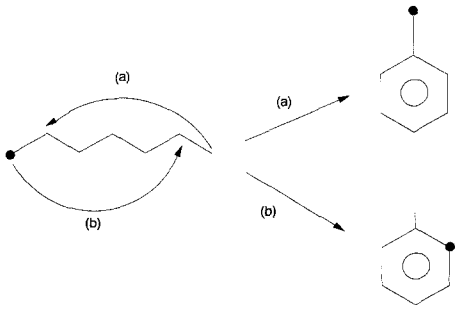

(10)

that lead to ^{13}C enrichment only at methyl and *ortho*-positions and to equal number of molecules with ^{13}C in the methyl and in the ring carbons. Enrichment at other carbon positions can occur in secondary isotopomerization of *ortho*-labeled toluene molecules by methyl group shifts:

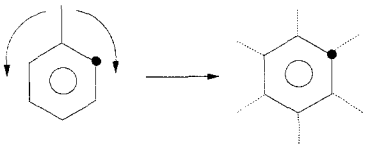

(11)

Such methyl shifts are consistent with the presence of acid sites on WC/O-800 K and with the well-established ability of acid catalysts to isomerize xylenes and other alkyl aromatics (*20*). Such isomerization reactions are limited by the rate of carbenium-

ion formation and lead to equilibrated isomeric distributions. Therefore, we expect that isotopomerization of ring-labeled toluene would place ^{13}C at random ring positions but would not exchange ^{13}C between methyl and ring carbons. The observed ^{13}C distribution in toluene is consistent with predominant (1,6) ring closure; a fraction of the primary toluene products then undergoes methyl shifts within the contact time of our experiment.

Ring closure can involve acid-catalyzed intramolecular coupling reactions (*14*):

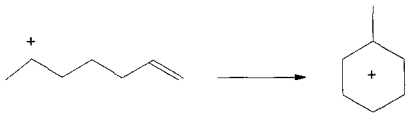

(12)

However, competing pathways

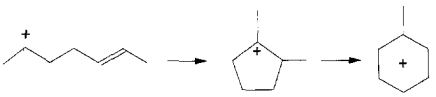

(13)

would lead to ^{13}C exchange between methyl and ring position and to an abundance of toluene molecules with ^{13}C in ring rather than methyl carbons.

An alternate mechanism involves thermal electrocyclic addition reactions of *cis*-heptatriene molecules (*21–23, 10*):

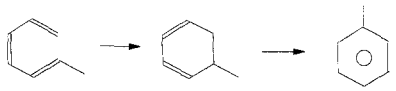

(14)

Conjugated heptatrienes lead exclusively to methyl and *ortho*-enrichment with equal probability (*10*). Nonconjugated heptatrienes cyclize via unstable bicyclospecies and lead to enrichment at *meta-*, *para-*, and *ortho*-carbons. Nonconjugated heptatrienes are less stable than conjugated isomers; thermodynamic calculations show that nonconjugated heptatrienes account for about 4% of the isomers capable of cyclization (*cis*-isomers) at 723 K (*10*). Such dehydrocyclization pathways require only dehydrogenation sites and do not involve surface ring-closure steps; they account for cyclization reactions on Te- and Cr-based catalysts (*10, 21–23*).

The isotopomer distribution predicted from thermal cyclization of an equilibrated mixture of conjugated and nonconjugated heptatrienes is shown in Table 6 (Column 2). If 25% of the toluene molecules then isotopomerizes by rapid shifts of the methyl group to random positions, we obtain an isotopic distribution (Column 3, Table 6) that agrees well with our experimental data. The presence of alkane dehydrogenation sites, the absence of (1,5) ring-closure pathways, and the predominant (1,6) ring closure observed on WC/O-800 K also suggest that thermal cyclization reactions of heptatrienes account for the formation of toluene during *n*-heptane reactions at 723 K.

No unlabeled *n*-heptane or toluene were observed among the products of *n*-heptane-1-^{13}C reactions on WC/O-800 K at 723 K. Therefore, no exchange occurs between adsorbed reactants and ^{12}C atoms placed in the WC structure during carbide preparation or during its subsequent deactivation in unlabeled *n*-heptane reactions. These results suggest that carbon–carbon bond cleavage steps leading to C_1–C_6 hydrocarbons are irreversible, as also shown by the absence of doubly-labeled molecules and of C_8^+ hydrocarbons among reaction products.

3.11 Deuterium Exchange and Kinetic Isotope Effects in n-Heptane Reactions in WC/O-800 K

WC/O-800 K catalyzes the exchange of deuterium atoms into unreacted *n*-heptane (C_7H_{16}) and its reaction products (Fig. 9). Deuterium exchange into *n*-heptane probes the reversibility of the initial *n*-heptane dehydrogenation step and the number of C–H bonds that are activated during *n*-heptane surface sojourns.

All products of C_7H_{16}/D_2 mixtures are highly deuterated, suggesting that most C–H bonds in reacting molecules interact with the surface during one turnover (Fig. 9). Toluene molecules quickly reach com-

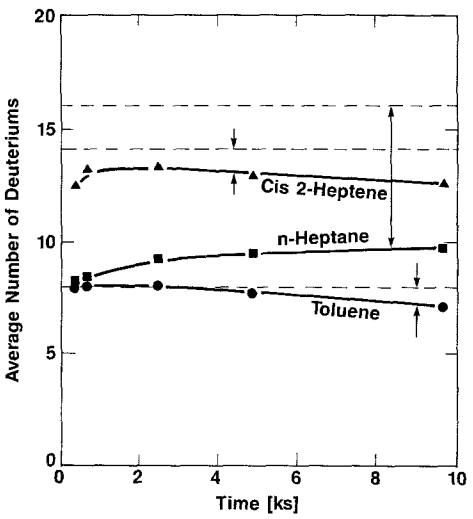

FIG. 9. Deuterium content in *n*-heptane/D_2 reaction products (723 K, 4.4-kPa *n*-heptane (C_7H_{16}), 96-kPa D_2, 2.9–15.1% *n*-heptane conversion).

plete deuteration (d_8) and then slowly acquire a few protium atoms as protium atoms from reacting *n*-heptane dilute the deuterium gas phase. Heptenes also reach almost complete deuteration very quickly. The product deuterium content is higher than that in *n*-heptane, either because of the long surface residence time required to form them or because of their higher reaction probability in secondary deuteration reactions. *n*-Heptane, however, is also extensively deuterated; the total number of deuterated *n*-heptane molecules is higher than expected from the rate of heptene hydrogenation events in the partially reversible initial dehydrogenation. Such hydrogenation events are expected to introduce hydrogen or deuterium atoms from a surface pool equilibrated with the predominantly deuterium gas phase.

The distributions of deuterium in *n*-heptane and in *cis*-2-heptene molecules are shown in Fig. 10. Three types of deuterated species are present. A part of the distribution centered about d_{12}–d_{14} appears in both *n*-heptane and heptene; it probably arises from extensive secondary exchange of reactive heptenes, which, when deuterated to *n*-heptane, give rise to similar features in the *n*-heptane deuterium distribution. The fraction of the *n*-heptane molecules contained within this part of the distribution increases with contact time. The deuterium content in this feature obeys a binomial distribution, consistent with equilibration of heptene molecules with a surface pool that is mostly deuterium. The deuteration turnovers for the d_8–d_{16} fraction reflect the rate of heptene "hydrogenation" steps; they are defined as the number of *n*-heptane molecules containing more than eight deuterium atoms per surface site. The ratio of deuteration to *n*-heptane conversion turnover rates extrapolates to a value of 3.2 at zero contact time, a value qualitatively higher than that obtained at 723 K using ^{13}C isotopic tracers (2.1, Fig. 4c).

A second feature in the deuterium distribution appears between d_2 and d_7; its presence in *n*-heptane is hidden by overlap with the two other features in the distribution. It apparently arises from primary heptene products before they exchange further in secondary reactions; its contribution is unaffected by residence time, suggesting that they are reactive intermediate species that are continuously formed in primary reaction steps and subsequently converted to more deuterated products in secondary reactions. The third feature appears only in *n*-heptane and corresponds to sequential single-exchange events; it contains d_1–d_4 species and probably arises from reversible dissociative adsorption of *n*-heptane. In effect, the *n*-heptane dehydrogenation step is partially traversed and desorption occurs by hydrogenation of adsorbed species before the generation of gas-phase heptene products. Thus, *n*-heptane can also chemisorb reversibly on WC/O-800 K without extensive dehydrogenation. The fraction of the deuterated *n*-heptane contained within this feature first increases, but then reaches a steady-state value as it continues to undergo dehydrogenation and deuteration reactions with increasing contact time.

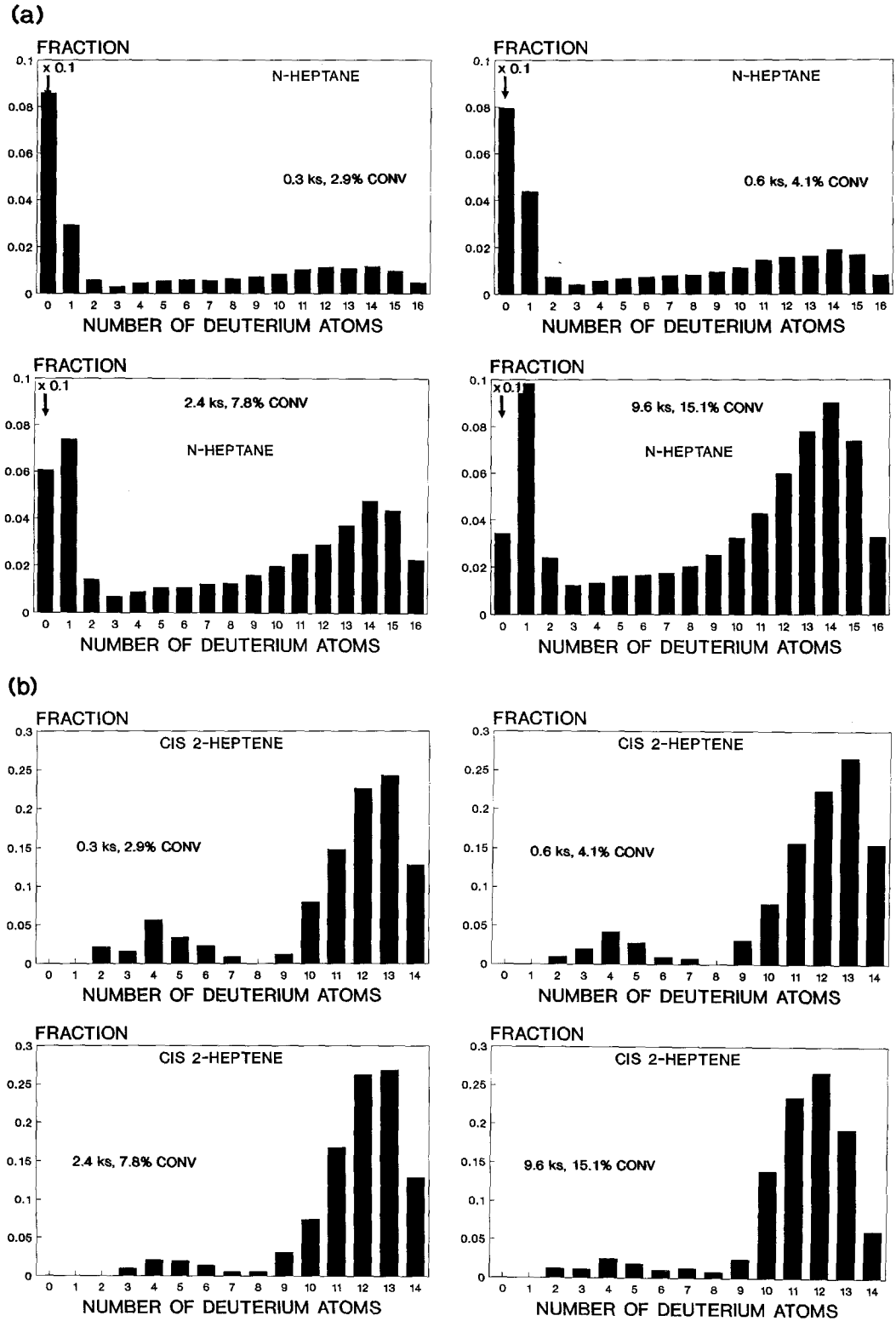

FIG. 10. Deuterium distribution in *n*-heptane/D_2 reaction products: (a) unreacted *n*-heptane, (b) *cis*-2-heptane (723 K, 4.4-kPa *n*-heptane (C_7H_{16}), 96-kPa D_2, 2.9–15.1% *n*-heptane conversion).

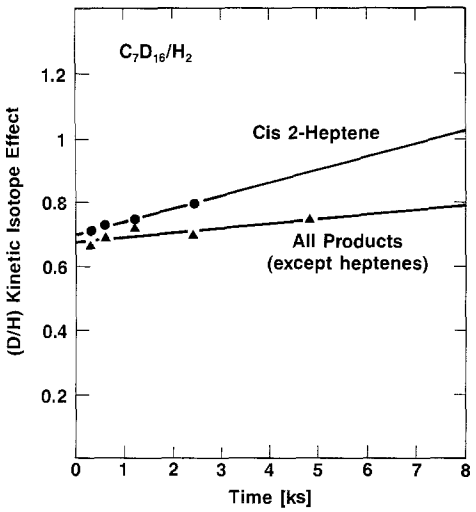

FIG. 11. Kinetic isotope effects in C_7D_{16}/H_2 and C_7H_{16}/H_2 Reactions on WC/O-800 K. (723 K, 4.4-kPa *n*-heptane (C_7H_{16} or C_7D_{16}), 97-kPa hydrogen).

Kinetic isotope effects (H/D) for the conversion of *n*-heptane on WC/O-800 K at 723 K were also measured. They are defined as the ratio of turnovers for individual products of C_7D_{16}/H_2 and C_7H_{16}/H_2 mixtures. The conversion rate of perdeuterated *n*-heptane to stable products (toluene, isoheptanes, and C_1–C_6) is slower than that of undeuterated *n*-heptane (Fig. 11). The kinetic isotope effect (KIE) extrapolates to 0.68 at zero contact time for stable products, a value very similar to that obtained for heptene formation (0.72). KIE values approach unity at higher contact times because of increasing protium exchange into reacting molecules. The similar initial values for heptene turnovers and for the formation of stable products suggest that *n*-heptane dehydrogenation is one of the rate-limiting steps in the catalytic sequence at 723 K.

These KIE values are similar to those obtained for *n*-heptane dehydrogenation reactions on Pt- and Te-based catalysts (*17*). However, they differ significantly from KIE values obtained for stable product formation on these catalysts. On Pt, KIE values for product formation are greater than unity (1.5–1.7) and deuteration actually increases the rate of *n*-heptane dehydrocyclization. On Te catalysts, KIE values are much less than unity (0.23); they reflect the need for several consecutive rate-limiting hydrogen desorption steps during toluene formation (*17*). In contrast, *n*-heptane reactions on WC/O-800 K are *initially* limited by C–H cleavage events in dehydrogenation steps at 723 K and not by hydrogen desorption or by subsequent reactions of heptenes. As contact time and heptene concentrations increase, both heptene reactions and *n*-heptane dehydrogenation limit overall reaction rates.

4. CONCLUSIONS

Our studies suggest that alkane rearrangements proceed via methyl-shift rearrangements of alkene intermediates on tungsten carbides modified by chemisorbed oxygen (WC/O-800 K). Isomerization products of 3,3-dimethylpentane and methylcyclohexane probe reactions support these conclusions and suggest the presence of acid sites that isomerize alkenes at 623 K with high selectivity.

At 623 K, *n*-heptane conversion rates are limited by reactions of intermediate heptenes on WO_x acid sites and not by the initial dehydrogenation step that forms heptenes on WC_x sites. The low ^{13}C content in isoheptanes and in other products of *n*-heptane-1-^{13}C/ 1-heptene mixtures shows that they are not formed by direct reactions of *n*-heptane. Isotopic enrichment occurs only at terminal carbons in isoheptanes formed from *n*-heptane-1-^{13}C reactants; thus, isomerization occurs predominantly via methyl shifts and not by hydrogenolysis of cyclic intermediates.

Isomer distributions in *n*-heptane and 3,3-dimethylpentane products formed on WC/O-800 K and on $Pt/WO_3 \cdot Al_2O_3$ are similar and consistent with methyl-shift isomerization pathways. Isolated WO_x species on tungsten carbide surfaces catalyze carbenium-ion reactions on Brønsted acid sites similar to those introduced by tetrahedral WO_x species on Al_2O_3. Oxygen-modified tungsten carbides, however, lack cyclization surface sites.

At higher temperatures (723 K), tungsten carbides deactivate rapidly, apparently by selective poisoning of WO_x sites. C_1–C_6 alkanes become the most abundant *n*-heptane conversion products. Dehydrogenation steps become increasingly rate-limiting at higher temperatures because their activation energy is lower than that for heptene conversion; as a result, steady-state heptene concentrations are below equilibrium. Isotopic tracers also show that dehydrogenation steps become increasingly rate-limiting at higher temperatures and that isomerization, dehydrocyclization, and hydrogenolysis also proceed via heptene intermediates at 723 K.

Dehydrocyclization occurs with low selectivity on WC/O-800 K; the toluene isotopomer distribution in *n*-heptane-1-^{13}C reaction products is consistent with thermal cyclization of heptatriene intermediates followed by acid-catalyzed migration of the methyl group. Such ring-closure pathways require only a dehydrogenation surface function. Deuterium exchange and kinetic isotope effect measurements show that hydrogen adsorption–desorption steps are fully equilibrated during *n*-heptane reactions. They suggest strong adsorption of reaction products and activation of several C–H bonds in one surface sojourn. Kinetic isotope effects (H/D) are less than unity and similar for *n*-heptane dehydrogenation steps and for the overall conversion reaction.

ACKNOWLEDGMENTS

The authors thank Dr. Kenneth D. Rose (Exxon) for the ^{13}C NMR experiments and Dr. Stuart L. Soled (Exxon) for helpful discussions on the acidity of WO_x surface species. We also thank Dr. Gerhard Raffeis (Stanford) for the preparation of the WC/O-800 K and Dr. John L. Robbins (Exxon) for his assistance in the synthesis of *n*-heptane-1-^{13}C.

REFERENCES

1. Levy, R. B., *in* "Advanced Materials in Catalysis" J. J. Burton and R. L. Garten, Eds.), pp. 101–127. Academic Press, New York, 1977.
2. Oyama, S. T., and Haller, G. L., *in* "Catalysis Spec. Per. Reports," Vol. 5, pp. 333–365. Royal Soc. Chem., London, 1982.
3. Leclerq, L., *in* "Surface Properties and Catalysis by Non-Metals" (J. P. Bonnelle, B. Delmon, and E. Derouane, Eds.), p. 433. Reidel, Dordrecht, 1983.
4. Levy, R. B., and Boudart, M., *Science* **181,** 547 (1973).
5. (a) Gaziev, G. A., Samsonov, G. V., Kylon, O. V., Roginsky, S. Z., Forika, E. A., and Yanovskii, I. F., *Dokl. Akad. Nauk. SSSR* **140,** 863 (1961); (b) Leclerq, L., Provost, M., Pastor, H., Grimblot, J., Hardy, A. M., Gengembre, L., and Leclerq, G., *J. Catal.* **117,** 371 (1989); (c) Leclerq, L., Provost, M., Pastor, H., and Leclerq, G., *J. Catal.* **117,** 384 (1989); (d) Vidick, B., Lemaitre, J., and Delmon, B., *J. Catal.* **99,** 428 (1986).
6. Ribeiro, F. H., Dalla Betta, R. A., Boudart, M., Baumgartner, J. E., and Iglesia, E., *J. Catal.*, **130,** 86 (1991).
7. Ribeiro, F. H., Boudart, M., Dalla Betta, R. A., and Iglesia, E., *J. Catal.* **130,** 498 (1991).
8. Smith, J. M., "Chemical Engineering Kinetics," 3rd ed. McGraw–Hill, New York, 1981.
9. Benson, J. E., and Boudart, M., *J. Catal.* **14,** 704 (1965).
10. Iglesia, E., Baumgartner, J. E., Price, G. L., Rose, and Robbins, J. L., *J. Catal.* **125,** 95 (1990).
11. Price, G. L., and Iglesia, E., *Ind. Eng. Chem.* **28,** 839 (1989).
12. Ogata, E., Kayima, Y., and Ohta, N., *J. Catal.* **29,** 296 (1979).
13. Soled, S. L., McVicker, G. B., Murrell, L. L., Sherman, L. G., Dispenzierre, N. C., Hsu, S. L., and Waldman, D., *J. Catal.* **111,** 286 (1988).
14. Pines, H., "The Chemistry of Catalytic Hydrocarbon Conversions." Academic Press, New York, 1981.
15. Fajula, F., and Gault, F. G., *J. Catal.* **68,** 291 (1981); **68,** 312 (1981); **68,** 329 (1981).
16. Daage, M., and Fajula, F., *J. Catal.* **81,** 394 (1983); **81,** 405 (1983).
17. Iglesia, E., Baumgartner, J. E., and Price, G.L. *J. Catal.* accepted.
18. Gault, F. G., *in* "Advances in Catalysis" (D. D. Eley, H. Pines, and P. B. Weisz, Eds.), Vol. 30, p. 1. Academic Press, New York, 1981.
19. Anderson, J. R., MacDonald, R. I., and Shimoyama, Y., *J. Catal.* **20,** 145 (1971).
20. McCaulay, D. A., and Lien, A. P., *J. Am. Chem. Soc.* **74,** 6246 (1952).
21. Kazansky, B. S., Isagulyants, G. V., Rozengart, M. I., Dubinsky, Yu. G., and Kovalenko, L. I., *in* "Proceedings, 5th International Congress on Catalysis, Palm Beach, 1972" (J. W. Hightower, Ed.), p. 1277. North-Holland, Amsterdam, 1973.
22. Derbentsev, Yu, I., and Isagulyants, G. F., *Russ. Chem. Rev.* **38,** 714 (1969).
23. Paal, Z., Tetenyi, P., *Acta Chim. Acad. Sci. Hungar* **54,** 175 (1967); **55,** 273 (1968); **58,** 105 (1968).